Journal of Solid State Chemistry **162,** 237–242 (2001)
doi:10.1006/jssc.2001.9279, available online at http://www.idealibrary.com on IDEAL®

Crystal Structure, Thermal Behavior, and Luminescence of $BaZnCl_4$-II:Sm^{2+} and Comparision to $BaZnCl_4$-I:Sm^{2+}

Claudia Wickleder[1]

Institut für Anorganische Chemie, Universität zu Köln, Greinstrasse 6, D-50939 Köln, Germany

Received February 26, 2001; in revised form June 6, 2001; accepted June 12, 2001

IN HONOR OF PROFESSOR PAUL HAGENMULLER ON THE OCCASION OF HIS 80TH BIRTHDAY

Slightly different reaction conditions lead to two modifications of single crystalline $BaZnCl_4$. The crystal structure of $BaZnCl_4$-II (orthorhombic, *Pbcn* (No. 60), $Z = 4$, $a = 6.5041(9)$, $b = 15.363(3)$, $c = 6.819(1)$ Å, $R_{all} = 0.0608$) consists of edge and corner sharing $[BaCl_8]$ polyhedra with $[ZnCl_4]$ tetrahedra filling the holes of the $[BaCl_8]$ network. The polyhedra in $BaZnCl_4$-I are nearly equal but the linkage is different. Both modifications can be obtained as single phases from $BaCl_2/ZnCl_2$ mixtures and show no phase transitions down to 4 K. Emission spectra of both modifications doped with Sm^{2+} reveal $4f^5 5d^1 \rightarrow {}^7F_J$ as well as ${}^5D_0 \rightarrow {}^7F_J$ transitions. In spite of the similar surrounding of Sm^{2+} in both modifications the shift of the maximum of the $d \rightarrow f$ emission is 450 cm^{-1}, showing that small changes in the coordination polyhedra of divalent rare earths cause large changes in luminescence properties.

Key Words: **tetrachlorozincates; thermal behavior; divalent lanthanides; samarium; luminescence.**

INTRODUCTION

Luminescence of divalent europium is used in some areas of application: $BaMgAl_{10}O_{17}:Eu^{2+}$, $Sr_5(PO_4)_3Cl:Eu^{2+}$, and $Sr_2Al_6O_{11}:Eu^{2+}$ are applied as blue phosphors in the energy-saving three-color lamps, and $BaFBr:Eu^{2+}$ is a well known X-ray storage phosphor (1). The efficiency of the parity allowed $4f^n5d^1 \rightarrow 4f^{n+1}$ transitions can be quite high. The energy, the bandwidth, and the thermal quenching of the emission depends on the position of the lowest $4f^n5d^1$ excited state relative to the $4f^{n+1}$ ground state. Both, the energy difference, ΔE, and the shift of the equilibrium of the metal–ligand distances, Δr_0, are of importance (Fig. 1). These two items depend strongly on various parameters of the crystallographic site of the host lattice-like metal–ligand distance, covalency, coordination number, and site symmetry. A small site with ionic ligands causes a large crystal field strength and a large crystal field splitting, resulting in a small ΔE and a low energetic emission, but Δr will be small in this case, shifting the emission to higher energy. If the covalency is small, low energetic emission is observed, known as the nephelauxetic effect (2). Other important parameters are the polarization of the ligand due to the second coordination sphere (3), and the position of the conduction band of the host lattice (4).

The exact influence of these parameters is difficult to determine. In general, changing the host lattice will change most of them. For a systematic investigation it would be advantageous to have similar host lattices with only one of the mentioned parameters changing.

The crystal structure of $BaZnCl_4$-I (5) and preliminary results of luminescent investigations of $BaZnCl_4$-I:Sm^{2+} (6) have been reported recently. It has been shown that the Sm^{2+} ions substitute only Ba^{2+} ions of the host lattice which are located on sites with the point symmetry C_2. In this work, the crystal structure of a second modification of $BaZnCl_4$, $BaZnCl_4$-II, is presented, as well as the phase behavior of the two modifications. Room temperature emission spectra of both modifications doped with Sm^{2+} ions are discussed. Emission spectra of $BaZnCl_4:Sm^{2+}$ at lower temperature as well as excitation spectra and lifetime investigations will be reported elsewhere.

EXPERIMENTAL SECTION

Two modifications of $BaZnCl_4$ were prepared from the binary chlorides $BaCl_2$ (Merck, p.a.) and $ZnCl_2$ (Merck, p.a.). The educts were dried under vacuum at 150°C and sublimed at 1000 and 400°C, respectively. For the synthesis of $BaZnCl_4$-I the educts were heated in an evacuated silica ampoule at 600°C for 10 h followed by slow cooling (1°C/h) using the Bridgman technique. $BaZnCl_4$-II was obtained analogously but the maximum temperature was only 480°C. Both modifications crystallize as big colorless crystals of sizes up to $4 \times 4 \times 4$ mm^3. Due to their moisture sensitivity

[1] Fax: 0049-(0)221-470-5083. E-mail: claudia.wickleder@uni-koeln.de.

0022-4596/01 $35.00

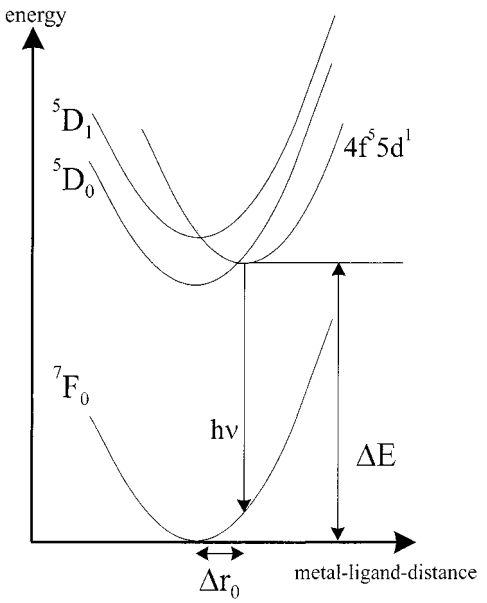

FIG. 1. Schematic configurational coordinate diagram of Sm^{2+}. ^7F_J levels ($J = 1$–6) are omitted for clarity. The arrow downwards indicates the $d \rightarrow f$ emission energy, ΔE, the energy difference between the parabola, and Δr_0, the difference of the equilibrium metal–ligand distance of the opposite parity states.

they have to be handled under inert conditions in an argon-filled glove box.

According to temperature-dependent powder X-ray diffraction measurements using a powder diffractometer (Stoe & Cie, Stadi P) equipped with a closed-cycle helium cryostat both modifications were single phase at room temperature. No phase transition was detected for both samples down to 40 K.

For crystal structure determinations of $BaZnCl_4$-II at 293 and 140 K small crystals of about 0.1 mm in diameter were mounted in glass capillaries using a polarizing microscope. The scattering intensities were collected with an imaging-plate-diffractometer (Stoe & Cie) equipped with a cryostat (Oxford Instruments). Structure solution and refinement were successful in space group *Pbcn* (No. 60) using the programs SHELXS86 and SHELXL93 (7), respectively. A numerical absorption correction was applied after optimization of the crystal shape (programs X-RED and X-SHAPE (8)). The crystallographic data and the parameters of their determination are given in Tables 1–3. The crystal structure of $BaZnCl_4$-I was reported recently (5).

DSC/TG investigations were performed using a STA 409 thermal analyzer (Netzsch). For that purpose about 10 mg of the substances were filled in corundum containers and heated with a constant rate of 10 K/min under flowing argon. The thermal decomposition was followed from 30 up to 800°C. For the DSC data a baseline correction was applied. Characteristic points like start and end temperatures of the thermal effects were taken from the differentiated DSC curve following common procedures (11).

For luminescence measurements big crystals of $BaZnCl_4$:Sm^{2+} (0.05%) of both modifications were grown. To avoid lattice distortions as well as mixed valencies when doping Sm^{3+} into the samples followed by a reduction of the trivalent state another route was used. First, $SmCl_3$ was prepared from Sm_2O_3 (99.999%, alpha) using the ammonium halide route (12). $SmCl_2$ was obtained by the reduction of $SmCl_3$ with Sm metal (99.99%, alpha) in a molar ratio of 2:1 at 900°C in a tantalum container. The purity of the product was checked by powder diffraction meaurements. For the synthesis of $BaZnCl_4$:Sm^{2+} in tantalum containers, $SmCl_2$ was added to the binary chlorides in

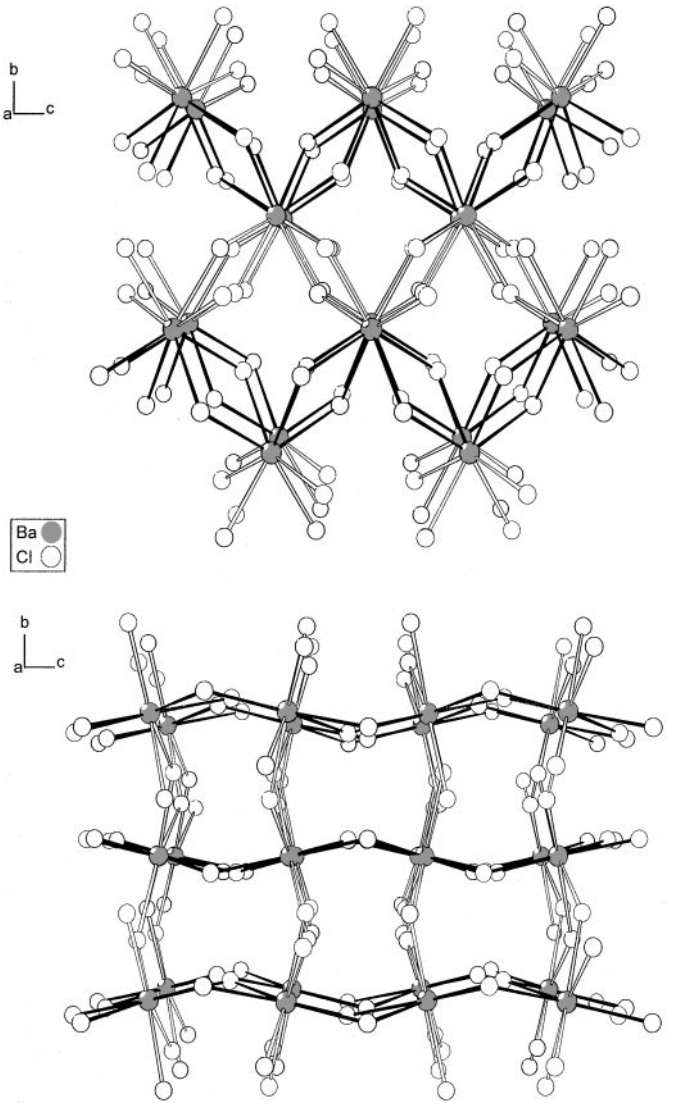

FIG. 2. Linkage of the [$BaCl_8$] polyhedra in the crystal structure of $BaZnCl_4$-II (top) and $BaZnCl_4$-I (bottom). Bonds to Cl^- ions involved in edge sharing are emphasized in black.

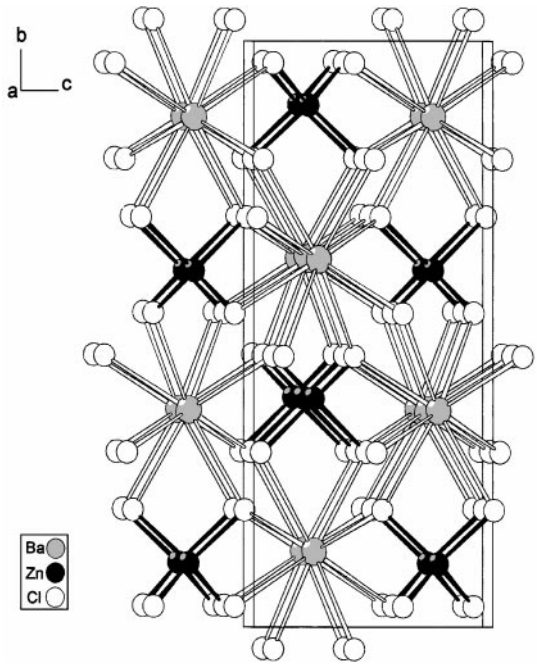

FIG. 3. Crystal structure of $BaZnCl_4$-II viewed along [100]. Zn^{2+}–Cl^- bonds are shown in black.

a molar ratio of 0.05%. $BaZnCl_4$-I:Sm^{2+} is weak red-brownish, while $BaZnCl_4$-II:Sm^{2+} is slightly pink. Due to their moisture sensitivity, the specimens have to be sealed in silica ampoules.

Emission spectra at room temperature were recorded using a frequency-doubled Nd:YAG laser (Spectra Physics, GCR 11, $\lambda = 532$ nm) as excitation source. The emission signal was focused on the entrance slit of a 0.27-m single monochromator and detected using a photomultiplier (Hamamatsu, R2949), a preamplifier (Stanford, SR445), and a photon counting system (Stanford, SR400). The spectra were corrected for photomultiplier sensitivity.

RESULTS AND DISCUSSION

Crystal Structures

$BaZnCl_4$-II crystallizes in the orthorhombic space group *Pbcn* and is isotypic to $UCrO_4$ (13). The crystallographic data at room temperature as well as at 140 K are given in Tables 1 to 3. The structure consists of [$BaCl_8$] polyhedra which can be grasped as trigon dodecahedra (point symmetry C_2). The Ba^{2+}–Cl^- distances range from 3.16 to 3.20 Å (Table 3) with four ligands being slightly closer to the Ba^{2+} ion (3.16 Å) than the other two (3.18 and 3.20 Å, respectively). The [$BaCl_8$] polyhedra are linked in two different ways: They share two common edges forming zig-zag chains along [001], and four common vertices connect the chains to a three-dimensional network (Fig. 2).

The Zn^{2+} ions are surrounded by four Cl^- ions with distances between 2.27 and 2.30 Å (Table 3) in the form of a tetrahedron. The angles within the tetrahedron are quite distorted. The tetrahedra fill the empty voids in the [$BaCl_8$] polyhedra network in such a way that each Cl^- ion connects to one Zn^{2+} and two Ba^{2+} ions (Figs. 2 and 3). Six [$ZnCl_4$] polyhedra are attached to one [$BaCl_8$] polyhedron via common corners; an additional polyhedron is linked via a common edge.

The coordination polyhedra of $BaZnCl_4$-I are very similar, but the linkage is different (5) (Fig. 2). There are also [$BaCl_8$] polyhedra in the form of trigonal dodecahedra with four different Ba^{2+}–Cl^- distances (3.140–3.190 Å, also point symmetry C_2) which are only a little smaller than in

TABLE 1
Data Collection Parameters and Crystallographic Data for $BaZnCl_4$-II (1, 293 K; 2, 140 K)

	1	2
Lattice parameters (Å)	$a = 6.5041(9)$	$a = 6.490(1)$
	$b = 15.363(3)$	$b = 15.374(2)$
	$c = 6.819(1)$	$c = 6.824(1)$
Molar volume (cm^3/mol)	102.6	102.5
No. of formula units (Z)	4	
Crystal system	Orthorhombic	
Space group	*Pbcn* (No. 60)	
Diffractometer	Stoe IPDS	
Radiation	Mo$K\alpha$ (graphite monochromator, $\lambda = 0.7107$ Å)	
Data range	$5° < 2\theta < 56°$	$4° < 2\theta < 56°$
Index range	$-8 \le h \le 8$	$-8 \le h \le 8$
	$-20 \le k \le 20$	$-19 \le k \le 19$
	$-8 \le l \le 9$	$-8 \le l \le 8$
Rotation angle range; φ-increment	$0° < \varphi < 250°$; $\Delta\varphi = 2°$	$0° < \varphi < 200°$; $\Delta\varphi = 2°$
No. of images	125	100
Exposure time	5 min	4 min
Detector distance	60 mm	60 mm
Data corrections	Polarization/Lorentz (8)	
Absorption corrections	Numerical, after crystal shape optimization (8)	
μ (cm^{-1})	107.0	107.0
No. of collected reflections	5764	5898
No. of unique reflections	828	825
No. of reflections with $I_0 > 2\sigma(I)$	559	595
R_{int}	0.1125	0.0763
Structure determination and refinement	SHELXS-86 and SHELXL-93 (7)	
Scattering factors	Intern. Tables, Vol. A (9)	
Goodness of fit	0.899	0.922
$R1$; w$R2$ $I_0 > 2\theta(I)$	0.0350; 0.0702	0.0328; 0.0781
$R1$; w$R2$ (all data)	0.0608; 0.0764	0.0507; 0.0842
Max/min final electron density	0.984/ − 1.680	0.959/ − 1.047
CSD No.	411951	411952

TABLE 2
Positional Parameters and Equivalent Isotropic Displacement Parameters for $BaZnCl_4$-II at 293 and *140 K*

Atom	Site	*x/a*	*y/b*	*z/c*	$U_{eq} \times 10^{-5}$ (Å^2)
Ba	4*c*	0	0.12940(3)	$\frac{1}{4}$	16.2(2)
Ba	*4c*	*0*	*0.12930(3)*	$\frac{1}{4}$	*12.8(2)*
Zn	4*c*	$\frac{1}{2}$	0.8908(1)	$\frac{1}{4}$	18.1(2)
Zn	*4c*	$\frac{1}{2}$	*0.89066(7)*	$\frac{1}{4}$	*13.6(2)*
Cl1	8*d*	0.2446(3)	0.9631(1)	0.4084(2)	25.1(4)
Cl1	*8d*	*0.2449(3)*	*0.9632(1)*	*0.4085(2)*	*18.2(3)*
Cl2	8*d*	0.1465(3)	0.2996(1)	0.0245(3)	27.7(4)
Cl2	*8d*	*0.1468(3)*	*0.2992(1)*	*0.0234(2)*	*20.2(4)*

Note. $U_{eq} = \frac{1}{3}[U_{11} + U_{22} + U_{33}]$ (10).

$BaZnCl_4$-II. The $[ZnCl_4]$ tetrahedron shows also two different distances Zn^{2+}–Cl^-. Analogously to $BaZnCl_4$-II, the $[BaCl_8]$ polyhedra are connected via two common edges and four common vertices, but here the edge-building Cl^- ions are opposite and not neighboring as in $BaZnCl_4$-II. Additionally, the $[BaCl_8]$ polyhedra are connected via two common edges and four common corners to six different $[ZnCl_4]$ tetrahedra.

Thermal Investigations

Two modifications of $BaZnCl_4$ can be synthesized which are pure phase according to X-ray powder diffraction measurements. Both modifications are obtained from the binary chlorides, $BaZnCl_4$-I at 600°C and $BaZnCl_4$-II at 480°C. No phase transition was detected when cooling down to 40 K from powder diffraction measurements. Additionally, luminescence measurements at 4 K prove the phase stability of both modifications. In 1914 Sandonnini presented a phase diagram of $BaCl_2$ and $ZnCl_2$ which shows only one incongruent melting modification of the composition $BaZnCl_4$ (14). However, no phase transition had been detected, so this phase diagram is not suitable to explain the results presented in this work.

TABLE 3
Selected Internuclear Distances (Å) and Angles (°) for $BaZnCl_4$-II at 293 and *140 K*

Ba–Cl_2 (2×)	3.159(2)	Cl_1–Zn–Cl_1	121.4(1)
Ba–Cl_2 (2×)	*3.153(2)*	*Cl_1–Zn–Cl_1*	*121.2(1)*
Ba–Cl_1 (2×)	3.159(2)	Cl_2–Zn–Cl_1	106.5(1)
Ba–Cl_1 (2×)	*3.159(2)*	*Cl_2–Zn–Cl_1*	*106.4* (1)
Ba–Cl_2 (2×)	3.179(2)	Cl_2–Zn–Cl_1	108.3(1)
Ba–Cl_2 (2×)	*3.182(2)*	*Cl_2–Zn–Cl_1*	*108.6(1)*
Ba–Cl_1 (2×)	3.197(2)	Cl_2–Zn–Cl_2	104.5(1)
Ba–Cl_1 (2×)	*3.197(2)*	*Cl_2–Zn–Cl_2*	*104.5(1)*
Zn–Cl_1 (2×)	2.272(2)		
Zn–Cl_1 (2×)	*2.270(2)*		
Zn–Cl_2 (2×)	2.288(2)		
Zn–Cl_2 (2×)	*2.297(2)*		

To investigate this unusual phase behavior, DSC/TG investigations were performed. Measurements of a sample of pure $ZnCl_2$ show a melting peak with a maximum at 325°C and a boiling peak, which starts at 535°C. This is not a boiling point for standard conditions, because the measurement was carried out under flowing argon. However, the conditions during the synthesis are also not standard conditions.

Thermal investigations of $BaZnCl_4$-II show the stability of the compound up to 468°C. Above that temperature, $BaZnCl_4$-II starts to melt. The melting peak has its maximum at 479°C. During the cooling process down to room temperature only the solidification peak with an onset at 460°C was detected. DSC/TG measurements of $BaZnCl_4$-I showed a different behavior. The same melting and solidification signals are found, but a single peak which starts at 366°C was observed additionally in the heating curve which did not appear upon cooling.

According to the DSC/TG results the following model of the phase behavior of $BaZnCl_4$ is possible: In contrast to the phase diagram (14) there exist two modifications of $BaZnCl_4$. $BaZnCl_4$-I, which is the thermodynamically stable modification at lower temperature, undergoes a phase transition to $BaZnCl_4$-II at 366°C. Upon cooling $BaZnCl_4$-II remains metastable, so that no phase transition to $BaZnCl_4$-I occurs. $BaZnCl_4$-II can be prepared from a 1:1 mixture of the binary chlorides. Because of the metastability it is stable down to low temperatures. If the temperature during synthesis exceeds 535°C some amount of $ZnCl_2$ (depending on the size of and the pressure inside the ampoule) evaporates and disappears from the reaction mixture. Now there is some excess $BaCl_2$ in the melt, so that the system can bypass the point of phase transition and $BaZnCl_4$-I will crystallize as a single modification. The last drops of the melt will yield $BaCl_2$ and $BaZnCl_4$-I, solidifying at the top of the grown crystals and are not taken as samples for luminescence measurements.

In contrast to the above described preparation methods $BaZnCl_4$-I can be obtained at lower temperature. If mixtures of the educts in a molar ratio of 6:4 ($BaCl_2$:$ZnCl_2$) are heated up to only 470°C, $BaZnCl_4$-I together with $BaCl_2$ was detected from powder diffraction patterns. This may be seen as a proof for the suggested mechanism.

Luminescence of $BaZnCl_4$-I:Sm^{2+} and $BaZnCl_4$-II:Sm^{2+}

Because of the ionic radii of the divalent ions, 1.56 Å for Ba^{2+} and 1.41 Å for Sm^{2+} in eightfold coordination and 0.74 Å for Zn^{2+} in fourfold coordination (15), at least at low doping concentrations the occupation of Sm^{2+} of the Ba^{2+} sites in $BaZnCl_4$ is much more probable than the occupation of the Zn^{2+} sites. For $BaZnCl_4$-I:M^{2+} (M = Eu, Sm,

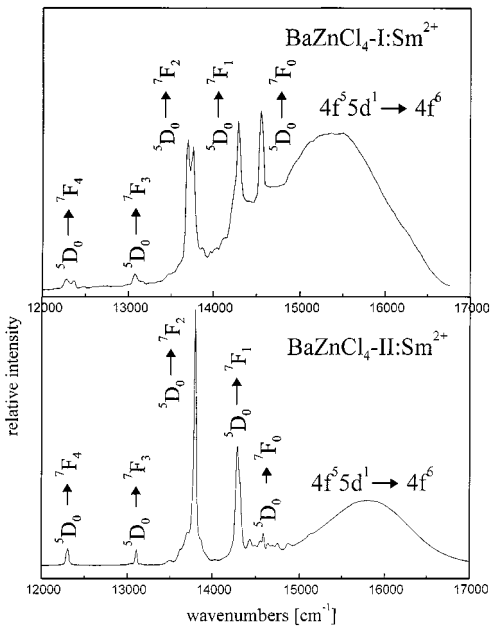

FIG. 4. Emission spectra of $BaZnCl_4$-I:Sm^{2+} and $BaZnCl_4$-II:Sm^{2+} at room temperature upon excitation at 18796 cm^{-1}. $^5D_0 \rightarrow {}^7F_J$ transitions are assigned. Note the difference of the $d \rightarrow f$ emission band between the two modifications.

Tm) (6) and $BaZnCl_4$-II:M^{2+} (M = Eu, Sm) luminescence measurements at 4 K show clearly that only one crystallographic site is occupied by M^{2+}. The number of crystal field levels of the ^7F_J states observed in the emission spectra of the Sm^{2+} doped compounds fit the site symmetry C_2. Because Ba^{2+} as well as Zn^{2+} ions occupy crystallographic sites with this symmetry the Sm^{2+} position cannot clearly determined.

The coordination number of eight and the point symmetry C_2 for the Ba^{2+} sites is equal in both modifications. The Ba^{2+}–Cl^- distances are approximately 1 pm longer in $BaZnCl_4$-II. The average distances are 3.159 Å ($BaZnCl_4$-I) (5) and 3.173 Å ($BaZnCl_4$-II) (Table 3), respectively. Thus, $BaZnCl_4$ is a very suitable system for studying the difference of the $d \rightarrow f$ emission of divalent lanthanide ions in very similar host lattices.

Figure 4 depicts the room temperature emission spectra of $BaZnCl_4$-I:Sm^{2+} (6) and $BaZnCl_4$-II:Sm^{2+} after $4f^6 \rightarrow 4f^55d^1$ excitation. In both spectra broad bands as well as sharp transitions are visible which can be assigned to $4f^55d^1 \rightarrow {}^7F_J$ and $^5D_0 \rightarrow {}^7F_J$ emissions of Sm^{2+} (Figs. 1 and 4). As expected, the $^5D_0 \rightarrow {}^7F_J$ emissions are at comparable energies in both modifications, while the $4f^55d^1 \rightarrow {}^7F_J$ emission of $BaZnCl_4$-II:Sm^{2+} shows a blue shift when compared to $BaZnCl_4$-I:Sm^{2+}. The maxima of the $d \rightarrow f$ emission bands are located at 15,350 cm^{-1} with $\Delta_{1/2} = 1450\ cm^{-1}$ (full width at half maximum, FWHM) ($BaZnCl_4$-I) and at 15,800 cm^{-1} with $\Delta_{1/2} = 1200\ cm^{-1}$ ($BaZnCl_4$-II). This shift of the maxima of 450 cm^{-1} is visible by eye after UV excitation. $BaZnCl_4$-I:Sm^{2+} shows a deep red luminescence while the luminescence of $BaZnCl_4$-II:Sm^{2+} is bright pink. The increasing Ba^{2+}–Cl^- distances in $BaZnCl_4$-II:Sm^{2+} cause a decreasing crystal field splitting of the d-levels of Sm^{2+} so that the lowest lying d-orbital is located at higher energy. Note that a very small change in the Ba^{2+}–Cl^- distances and a small change of the Cl–Ba–Cl angles lead to a drastic change in the energy of the $d \rightarrow f$ emission bands.

The simultaneous appearance of $f \rightarrow f$ *and* $d \rightarrow f$ emission shows that the lowest $4f^55d^1$ level is located at higher energy than the $^5D_0$ level. Because of thermal occupation of the $4f^55d^1$ level fast parity allowed $d \rightarrow f$ emission is visible. Due to the position of the lowest $4f^55d^1$ level relative to the $^5D_0$ level the thermal occupation in $BaZnCl_4$-II:Sm^{2+} is much lower as in $BaZnCl_4$-I:Sm^{2+}, resulting in a weaker $d \rightarrow f$ emission. Integration yields an intensity of $d \rightarrow f$ bands relative to the $f \rightarrow f$ peaks of 85% for $BaZnCl_4$-I:Sm^{2+} and 68% for $BaZnCl_4$-II:Sm^{2+}. At lower temperature only $f \rightarrow f$ transitions are visible in both modifications. The exact positions of the $4f^55d^1$ levels relative to the $^5D_0$ levels will be determined from temperature-dependent measurements.

The assignments of the $^5D_0 \rightarrow {}^7F_J$ transitions are also depicted in Fig. 4. They are similar to the emission peaks of the isoelectronic Eu^{3+} but due to the lower nuclear charge they are located at lower energy.

In opposite to $BaZnCl_4$-II:Sm^{2+}, $BaZnCl_4$-I:Sm^{2+} shows very strong $^5D_0 \rightarrow {}^7F_0$ emission, while $^5D_0 \rightarrow {}^7F_1$ is of comparable intensity. In Eu^{3+}-doped compounds the $^5D_0 \leftrightarrow {}^7F_0$ transition is very weak and strictly forbidden by electric and magnetic dipole selection rules. Some intensity is gained by J mixing (16). The $^5D_0 \leftrightarrow {}^7F_1$ transition in Eu^{3+} and Sm^{2+} is forbidden by both Judd–Ofelt and Wybourne–Downer mechanisms, and its appearance in the spectra is due to an allowed magnetic dipole process (17). Therefore, the strength of this transition is nearly independent of the energy separation to higher opposite parity states and also of the crystal field strength. The squared matrix elements are nearly equal in magnitude, so this transition is suitable for comparing the spectra of Sm^{2+} in different host materials (17). In contrast, the intensity of the $^5D_0 \leftrightarrow {}^7F_0$ transition in Sm^{2+} depends strongly on the position of the odd-parity $4f^55d^1$ states. The large increase of the $^5D_0 \rightarrow {}^7F_0$ emission in $BaZnCl_4$-I:Sm^{2+} might be due to the close position of the odd parity states relative to $^5D_0$ and $^7F_0$. The integrated intensity of the $^5D_0 \rightarrow {}^7F_2$ emission is similar in both spectra but the relative intensity of the individual crystal field lines is different as is observable at low temperature. This will be discussed elsewhere.

ACKNOWLEDGMENT

I am indebted to Professor Dr. G. Meyer for his generous support. Tables of crystal data and structure refinement, atomic coordinates and

equivalent displacement parameters, bond lengths and angles, as well as anisotropic displacement parameters are available from the Fachinformationszentrum Karlsruhe, D-76344 Eggenstein-Leopoldshafen (crysdata@FIZ-Karlsruhe.de) by giving the Deposition Numbers CSD.411951 and 411952.

REFERENCES

1. G. Blasse and B. C. Grabmaier, "Luminescent Materials," Springer-Verlag, Berlin, 1994.
2. G. Blasse, *J. Solid State Chem.* **4,** 52 (1972).
3. G. Blasse, *Eur. J. Solid State Inorg. Chem.* **33,** 175 (1996).
4. G. Blasse, *Photochem. Photobiol.* **52,** 417 (1990).
5. C. Wickleder, S. Masselmann, and G. Meyer, *Z. Anorg. Allg. Chem.* **625,** 507 (1999**)**.
6. C. Wickleder, *J. Alloys Compds.* **300,** 193 (2000).
7. G. M. Sheldrick, "SHELXS86 and SHELXL93: Programs for Solution and Refinement of Crystal Structures." Göttingen, 1986/1993.
8. (a) Fa. STOE & Cie, "X-RED 1.07: Data Reduction for STADI4 and IPDS." Darmstadt, 1996. (b) Fa. STOE & Cie, "X-SHAPE 1.01: Crystal Optimisation for Numerical Absorption Correction." Darmstadt, 1996.
9. Th. Hahn (Ed.), "International Tables for Crystallography." Vol. A. Reidel, Dordrecht/Boston, 1983.
10. R. X. Fischer and E. Tillmanns, *Acta Crystallogr. C* **44,** 775 (1988).
11. W. F. Hemminger and H. K. Cammenga, "Methoden der Thermischen Analyse." Springer-Verlag, New York, 1989.
12. G. Meyer, *Inorg. Synth.* **22,** 1 (1983).
13. M. Bacmann, E. F. Bertraut, and G. Bassi, *Bull. Soc. Franc. Mineral Cristallogr.* **88,** 214 (1965).
14. C. Sandonnini, *Gazz. Chim. Ital.* **44I,** 353 (1914).
15. R. D. Shannon and C. T. Prettwitt, *Acta Crystallogr. B* **25,** 925 (1969); R. D. Shannon, *Acta Crystallogr. A* **32,** 751 (1976).
16. B. Henderson and G. F. Imbusch, "Optical Spectroscopy of Inorganic Solids." Clarendon Press, Oxford, 1989.
17. M. Tanaka and T. Kushida, *Phys. Rev. B* **53,** 588 (1996).